SUSCEPTIBILITY WEIGHTED IMAGING IN MRI

Basic Concepts and Clinical Applications

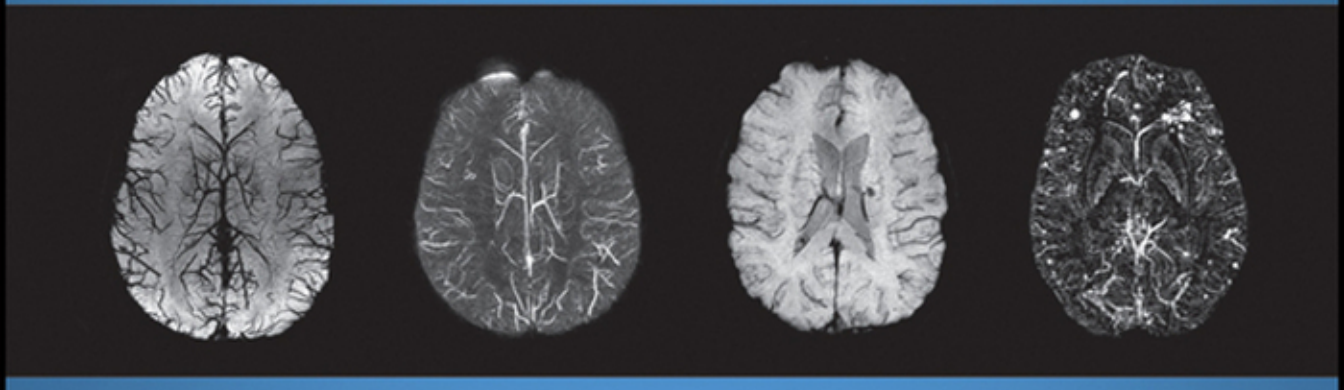

EDITED BY

E. MARK HAACKE

JÜRGEN R. REICHENBACH

WILEY-BLACKWELL

30

Functional Susceptibility Weighted Magnetic Resonance Imaging

Markus Barth and Daniel B. Rowe

INTRODUCTION

Functional magnetic resonance imaging (fMRI) based on the blood oxygenation level-dependent (BOLD) effect has found widespread applications in neuroscience and medicine since its detection in the early 1990s [1, 2] for its powerful ability to map brain regions that are "activated" during performance of a specific task. The functional contrast of fMRI is obtained by dynamically measuring the BOLD signal changes, using a time series of images to assess the hemodynamic response (e.g., blood flow, blood volume, and blood oxygenation). This is possible because changes in hemodynamics are linked to neural activity [3]. When neuron cells are active, oxygen consumption is increased, initially decreasing the oxygenation level in local capillaries. More importantly, this local increase in oxygen consumption leads to an increase in blood flow, delayed by approximately 1 2 s. Then as the increased blood flow is usually overcompensating the oxygen consumption with more than needed fresh blood, the oxygenation level will gradually increase again. This hemodynamic response reaches a peak after 4 5 s and then falls back to baseline (and typically forming an undershoot before returning to the baseline state). Consequently, the local concentrations of oxyhemoglobin and deoxyhemoglobin change dynamically due to the interaction between cerebral blood flow (CBF) and cerebral blood volume (CBV) [4].

Susceptibility Weighted Imaging in MRI, By E. Mark Haacke and Jurgen R. Reichenbach

The BOLD signal change amounts to

$$\frac{\Delta \mathrm{BOLD}}{\mathrm{BOLD}} = M \cdot \left(1 - \left(\frac{\mathrm{CMR_{O_2}}}{\mathrm{CMR_{O_2}}|_0}\right)^{\beta} \cdot \left(\frac{\mathrm{CBF}}{\mathrm{CBF_0}}\right)^{\alpha \ \beta}\right) \tag{30.1}$$

where

$$M \equiv \mathrm{TE} \cdot A \cdot \mathrm{CBV_0} \cdot [\mathrm{dHB}]^{\beta}_{v_0} \tag{30.2}$$

and

$$\frac{\mathrm{CBV}}{\mathrm{CBV_0}} = \left(\frac{\mathrm{CBF}}{\mathrm{CBF_0}}\right)^{\alpha} \tag{30.3}$$

where α is a constant that relates CBF changes to CBV changes, and $\mathrm{CBF_0}$ and $\mathrm{CBV_0}$ are the corresponding values at resting state. The parameter α has been determined experimentally as 0.38 [5] or 0.5 [6]. The parameter A is a field strength and sample-specific constant, and β is a constant in the range of 1 2 depending on the average blood volume [4].

Because oxyhemoglobin is diamagnetic while deoxyhemoglobin is paramagnetic, the interplay of the aforementioned hemodynamic processes results in a change in the magnetic susceptibility of blood, which in turn leads to a slight change in the local magnetic field and hence in the MR signal intensity. The MRI signal of blood is therefore dependent on the level of oxygenation that can be detected using an appropriate MR pulse sequence. The BOLD effect is commonly measured using the rapid acquisition of a series of 2D images with a contrast heavily weighted by the local field inhomogeneities, also known as T_2^*-weighted images. The most commonly used technique is called echo planar imaging (EPI), which is based on gradient echo acquisition. The EPI technique offers moderately good spatial and temporal resolution, covering the whole brain with a spatial resolution of about 3 mm and a temporal resolution of about 2 3 s. Recent technical advancements, such as the use of high magnetic fields ($\geq$3 T) and advanced "multichannel" RF reception, have increased the spatial resolution to the millimeter scale. Although the hemodynamic response takes several seconds, BOLD responses to temporally close stimuli (as close as 1 2 s) can be distinguished from one another, using experimental paradigms known as event-related fMRI. Using specifically designed MR pulse sequences, changes in CBF or CBV can also be measured.

THE VENOUS INFLUENCE ON THE FUNCTIONAL SPECIFICITY OF BOLD fMRI

The BOLD signal is mainly composed of signal contributions from larger veins, smaller venules, and capillaries, that is, where deoxyhemoglobin concentration change significantly. It has been shown that larger venous vessels give rise to a significant portion of the observed BOLD activation in both gradient echo [7 13] and spin echo fMRI [14]. This can lead to spurious activations and an intrinsic ambiguity of the actual localization of the neuronal activation and as a result reduce the functional specificity of fMRI. Using BOLD fMRI this problem cannot be solved by simply increasing the imaging spatial resolution [11]. However, experimental results indicate that the BOLD signal can be weighted

TABLE 30.1 Blood velocity in vessels of various diameters

Type of Vessels	Velocity (mm/s)	Diameter (μm)
Capillaries	0.26 1.1	<10
Venules	0.18 4.2	10 60
Intracortical veins	>5	>60
Pial veins		25 250

Data are taken from measurements of cat cortex [17] and are consistent with estimates for human brain vessels given in physiology textbooks [47].

more toward the smaller vessels at higher magnetic fields [15], and hence closer to the activation sites. It has been estimated that about 70% of the BOLD signal arises from larger vessels at 1.5 T, while about 70% arises from smaller vessels at 7 T. Furthermore, the portion of the BOLD signal originating from the capillaries increases roughly as the square of the magnetic field strength, making higher field scanners favorable for improving fMRI on both localization and sensitivity.

As the venous part of the vasculature is relevant for BOLD fMRI, knowledge about venous vasculature is very important. From an anatomical point of view, venous vessels in the brain can be classified into several categories [16]: the large cortical cerebral veins that drain the hemispheres, the (extracortical) pial venous network that drains the lobules, and the intracortical vascular network. The diameters of venous vessels span a vast range, from the very small venules (10 μm diameter) to the large sagittal sinus (diameter >10 mm; see Table 30.1 for a summary of some vessel properties [17]). The venules that drain the capillary bed and run approximately parallel to the cortical surface are part of the intracortical vascular network. The venules in turn are connected to intracortical veins that can be divided into several groups depending on from which cortical layer they are draining (Figure 30.1) [16]. For fMRI it is important that, these intracortical veins (diameter ~80 μm) emerge from the cortex roughly at a right angle to the pial vein (of diameter 200 500 μm) to which they then join. From the point of view of venous blood flowing, this means that

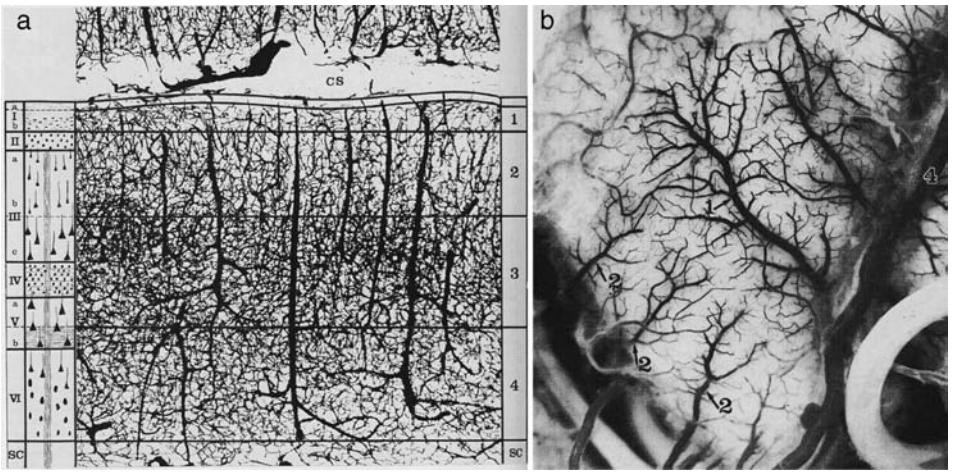

FIGURE 30.1 *Vascular architecture of the cortex. (a) The classification of the cortical layers (I VI) is given on the left-hand side and the vascular layers (1 4) on the right-hand side. (b) View on the cortical surface depicting the extracortical pial vein network. Reprinted from Ref. [16].*

venous blood is first drained within a layer to an intracortical vein that connects the vascular layers and leads to the cortical surface (Figure 30.1a). The venous blood then flows along the cortical surface draining away from the corresponding cortical area (Figure 30.1b). From this anatomical argument, it becomes clear that functional signal changes detected in large extracortical veins can severely compromise functional localization and specificity. The same argument explains why a layer-specific activation can be found in BOLD fMRI once the resolution is sufficiently high [18]. Duvernoy et al. [16] also define a vertical vascular unit that is centered with a large intracortical vein (also called principal intracortical vein) and surrounded by a ring of arteries, and both together form a column-like appearance.

From the seminal papers of Ogawa that triggered the use of the BOLD effect in fMRI [1, 2], as well as from previous chapters (Chapters 1 through 5), we know that a large venous vessel will have heavily T_2^*-weighted signals. Therefore, it was thought that a certain amount of the functional signal change (i.e., "activation") could originate from large venous vessels. The problem is that the larger the vein, the farther away it is located from the brain area where the neuronal activation occurs. The estimates for the distance where "spurious activation" can still be detected range from roughly 4 mm [19] to three times that amount [20]. By using Monte Carlo simulations with a cylindrical vein model, Boxerman et al. [21] showed that a spin echo sequence is primarily susceptible to capillaries whereas a gradient echo sequence is most sensitive to larger veins (diameter $>10\,\mu$m, see Figure 30.2). However, because of the influence of the vascular geometry (e.g., vessel size, vessel distribution, and orientation of the vessel to B_0) on the venous signal, it is still difficult to estimate the exact amount of extracortical vein contribution. One could argue that spin echo sequences should be used in fMRI because they are more susceptible to the capillary bed, but this increase in specificity comes with a greatly reduced sensitivity (about a factor of 3) that is normally not favorable for fMRI experiments.

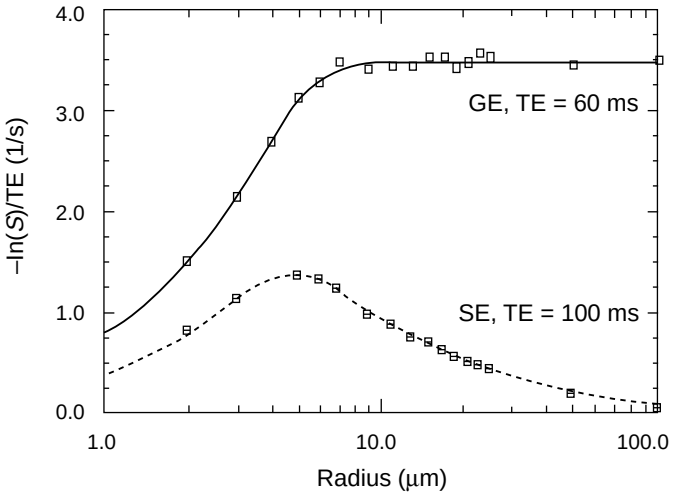

FIGURE 30.2 *Gradient and spin echo signals as a function of vessel radius. Reprinted with permission from Ref. [21].*

FUNCTIONAL SWI (fSWI)

To get a clearer view on the influence of veins on the BOLD fMRI signal, one can use the SWI technique to directly depict the venous vasculature in a functional experiment. Due to significant improvements in scanner hardware (e.g., high-field scanners, coil arrays) and imaging methods (e.g., parallel imaging), it is now possible to achieve very high isotropic resolution in functional MRI where veins can be identified and their contribution be estimated based on their spatial location rather than merely on model calculations [12]. As described in previous chapters, SWI can visualize very small veins (down to a diameter of 50 μm in human brain depending on field strength, see also Chapter 7) using very high-resolution 3D gradient echo imaging [22 24]. However, a very high spatial resolution is normally detrimental to fMRI experimental design and is difficult to implement. First, it will further increase the geometric distortion, making the registration of EPI data sets onto the anatomical or, in this case, the venographic data sets problematic. Second, the contrast of veins in high-resolution EPI is lower than in corresponding SWI data sets, most probably due to T_2^* blurring effects related to the long EPI readout. Nevertheless, some studies have attempted to identify veins [25 27] based on a rather coarse resolution at least in the slice direction (typically 3 5 mm). This leads to significant partial volume effects limiting the identification of small veins. However, once the functional signal characteristics (both magnitude and phase) are established in high-resolution studies, one can go back to lower resolution and try to use this information to reduce the influence of veins in a standard fMRI experiment. Therefore, attempts can be made to account for large vein effects by making use of their functional properties, for example, setting a threshold for the functional signal change [28] or using their phase behavior [29 32]. Other studies tried to reduce their influence by using diffusion weighting to at least remove the intravascular effects [33 35].

The SWI data were acquired at 3 T (Siemens Magnetom Trio, Siemens, Erlangen, Germany) with the following imaging parameters: TR/TE = 35/28 ms, flip angle = 15°, bandwidth = 100 Hz/pixel, voxel size = $0.75 \times 0.75 \times 0.75\,\text{mm}^3$, and GRAPPA with acceleration factor of 2. A custom-built eight-channel array coil (Stark Contrast; MRI Coils, Erlangen, Germany) was used in an fMRI experiment that was confined to the visual cortex (see Figure 30.3a for the positioning of the 3D slab) and was fast enough to be compatible with a block design. The stimulus paradigm consisted of a block showing a black screen with a fixation cross interleaved with a block showing a flickering checkerboard (5 Hz, that is, 200 ms for the full cycle). The block duration was matched to the respective acquisition times per 3D volume. These blocks were repeated between 14 and 37 times resulting in total acquisition times between 15 and 30 min per run. The data were analyzed using the general linear model as implemented in FEAT [36]. FSL MCFLIRT was used for motion correction between the volumes of the functional data set. No spatial or temporal smoothing was used.

Figure 30.3b shows one sample image from the functional data set. One can clearly see that the image in Figure 30.3b lacks the geometrical distortion that is common in EPI images, and it is also possible to directly identify venous vessels as dark spots or lines as a result of both dephasing between blood and tissue compartments in a voxel and extravascular effects [37, 38]. Veins could therefore be segmented manually or automatically [39] in the functional data sets based on their appearance.

With a block design visual task, the computed activation map clearly shows tubular structures that can be identified as veins by comparison with the venous vascular tree that is

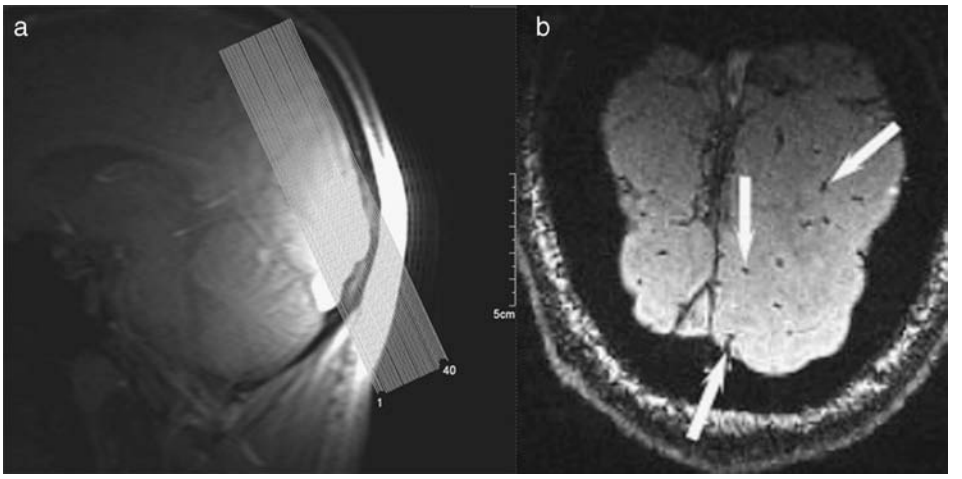

FIGURE 30.3 *(a) Positioning of the 3D slab on the sagittal localizer that clearly shows the high sensitivity region of the array coil on the occipital cortex. (b) Single slice out of functional data set (0.75 mm isotropic voxel size). Note the clear depiction of venous vessels (arrows). Reprinted with permission in a modified form from Ref. [13].*

segmented from the functional data itself (Figure 30.4a). A region of interest containing these segmented venous vessels is used as a mask to remove the respective voxels in the functional data set. In the second step, the general linear model will be applied again to these data sets with these visible veins removed. Due to the negligible geometric distortion, it is straightforward to overlay the significant activation on the corresponding anatomical slices after removing the venous effects (Figure 30.4b). The visible veins contributing to the activation volume was found to be approximately one quarter. The signal change maps (Figure 30.4c) can show the venous structures clearly. However, the venous vasculature differs significantly from subject to subject, suggesting a relationship and possible explanation to the intersubject variation of functional activation significance and localization that have been observed and confirmed by many studies, see also reference [40].

When analyzing the functional signal changes of the veins compared to cortical regions (Figure 30.5a), one finds that a huge signal change occurs in veins at high spatial resolution and gets closer to that of cortical regions with reduced resolution [11]. The signal changes in cortical regions are essentially independent of resolution. At a commonly used spatial resolution of about 4 mm voxel size, cortical activation and signal changes in veins are not distinguishable. However, with high enough resolution, a signal change threshold can clearly eliminate the majority of vein effects (Figure 30.5b). Such results also enable a rough estimation of how far the "activation" can travel along the draining veins by simply counting the voxels of the long tubular structures. The result of 40 50 mm is 10 times higher than expected from the original estimation of Turner [19] and still a factor of 3 higher than from Lauwers et al. [20]. One factor explaining such discrepancy is that an activated volume of only 1 cm^3 was assumed in their model, while the visual task used in the fSWI actually activates a much larger area. When performing a similar experiment at 7 T, one can still see the influence of veins (Figure 30.5c), that is, the appearance of high activation within the sulcus, but also activation in gray matter at the depth of cortical layer 4. This layer specific activation could also be demonstrated at 3 T, however, only by averaging over multiple cortical profiles [18].

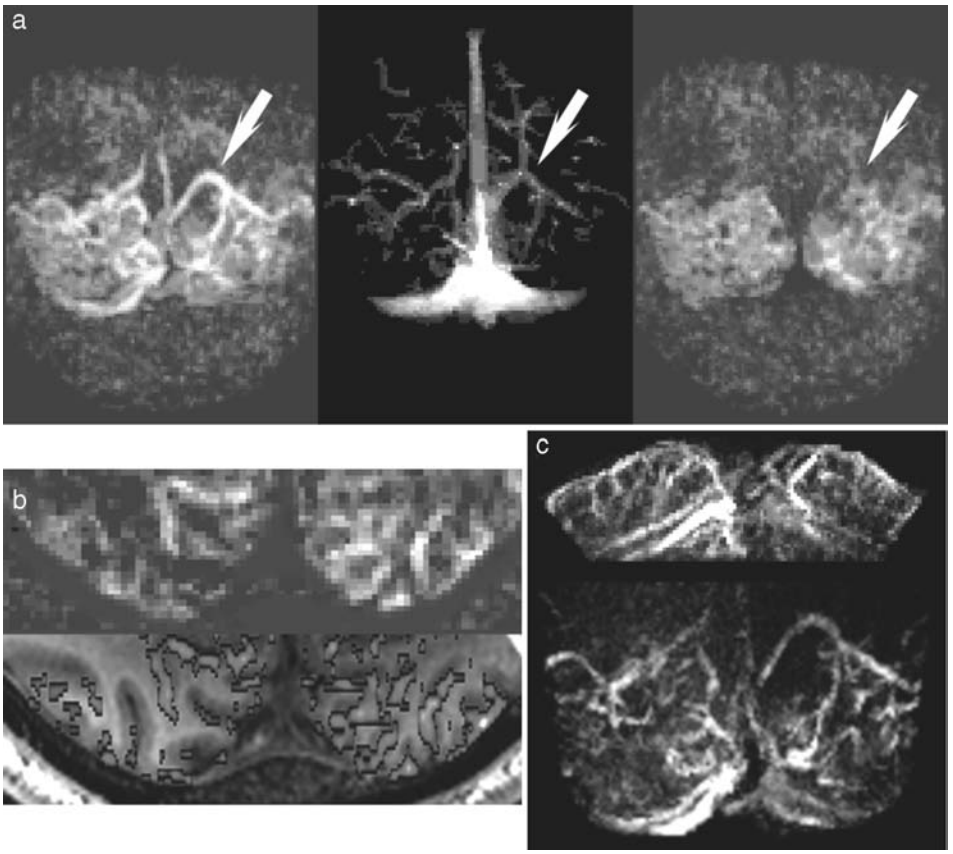

FIGURE 30.4 *(a) 3D z-map of the occipital lobe: before (left) and after (right) removing veins (middle: venous mask). (b) z-map of a single slice (upper) and its overlay on corresponding anatomical image (lower). (c) 3D signal change map of the same subject (upper: projection on axial plane; lower: projection on coronal plane). For visualization purposes, the resulting z-maps were smoothed; activated volumes are quantified before and after application of the venous mask by using all pixels in the z-maps above a threshold Z 2 and a cluster threshold of P 0.005. (a) and (b) reprinted with permission in a modified form from Ref. [13].*

SUSCEPTIBILITY-INDUCED PHASE CHANGES

Another confirmation of the influence of veins can be demonstrated with Figure 30.6. As discussed previously (see Chapters 2 and 4), venous vessels produce a phase effect due to dephasing between veins and surrounding tissue. This extravascular phase effect around a vessel has a specific cross-shaped pattern with two positive and two negative lobes which results in a dark cross in the magnitude and SWI image (Figure 30.6a and b). If the blood's susceptibility changes during activation, the extravascular phase distribution would also change accordingly; see, for example, Figure 30.6c where phase changes can be seen for some activated regions that are also seen in the magnitude. This phase information can be used to estimate oxygen saturation and its change during activation. In addition to the extravascular effect, the intravascular dephasing also changes the phase of a voxel containing blood and tissue. In cortical tissue where only small intracortical veins are

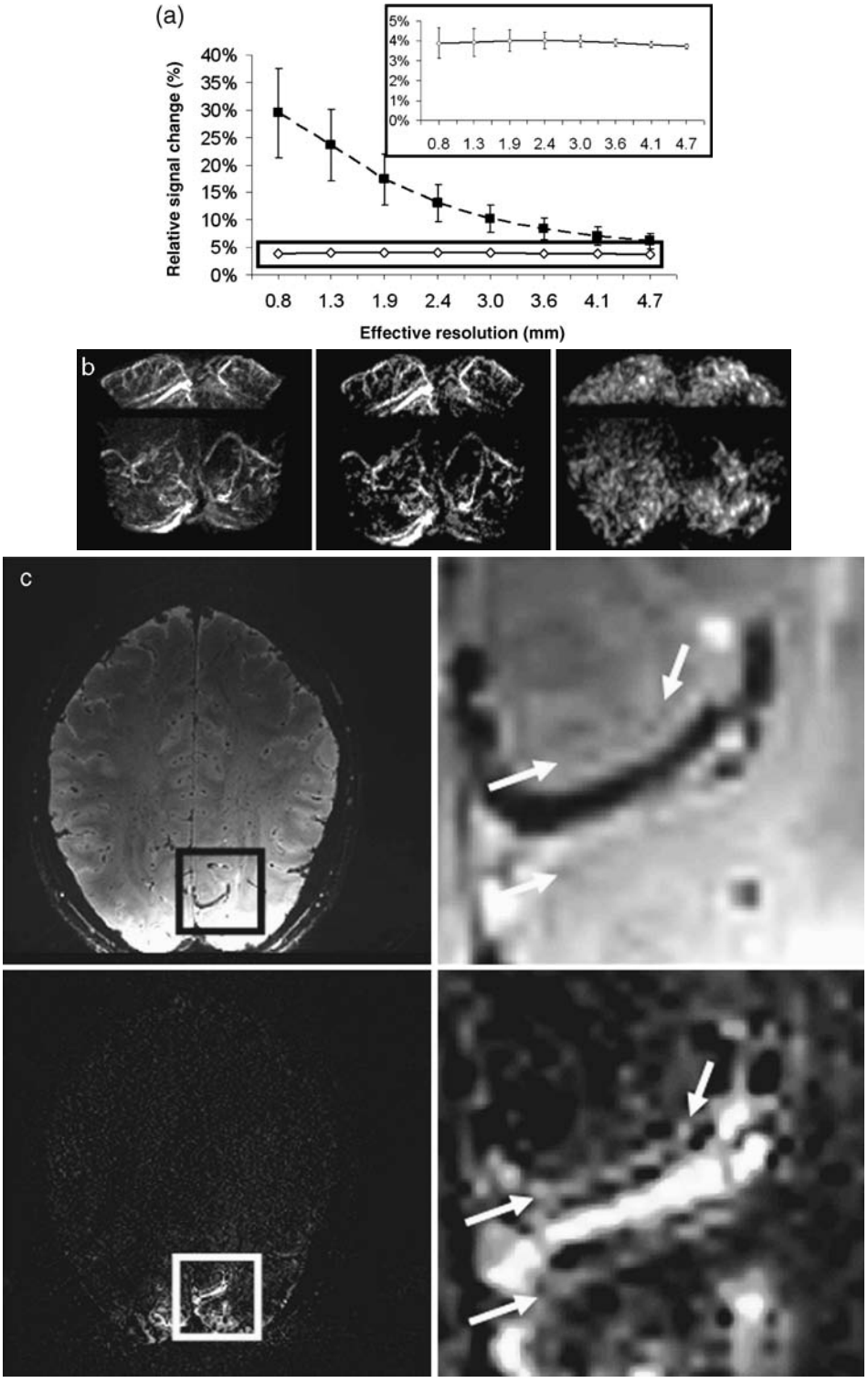
(a)
Relative signal change (%)
40%
35%
30%
25%
20%
15%
10%
5%
0%
0.8 1.3 1.9 2.4 3.0 3.6 4.1 4.7
Effective resolution (mm)
5%
4%
3%
2%
1%
0%
0.8 1.3 1.9 2.4 3.0 3.6 4.1 4.7
b
c

present, the extravascular phase effect averages out. Also, the intravascular dephasing effect will be very small, and assuming a random distribution of vessel orientations, it would be about 1/12 of that of a single vessel with the same blood volume. Because the venous blood volume in gray matter is very small (2 3%), a phase change in gray matter is difficult to detect experimentally. However, a very small phase effect has been observed in an animal study [41] and in a whole-brain analysis during breathing challenges [42].

The phase information is generally discarded in fMRI analysis and activations are computed using only the magnitude. However, the phase component of the data has been demonstrated to contain important spatial [22, 43] and temporal information [28, 41, 44] on neuronal activation-induced hemodynamics changes. In voxels containing mainly large veins change in oxygenation level will produce a change in phase assuming all other parameters are held fixed [45-47]. In voxels that contain mainly parenchymal tissue, the vessels are usually small and randomly oriented, and there will be little coherent task-related phase change (TRPC). In voxels that contain venous architecture (several millimeters or more) downstream from the site of neuronal firing, the vessels are usually larger and well oriented, thus producing a coherent task-related phase change [19], and in this way the phase component of the data contains information regarding the venous structure. It should be noted that the phase may also be contaminated by other physiological signals [48]. In fMRI, statistical activation analysis has predominantly utilized only the magnitude portion of the data, but more recently activation methods have been developed to utilize the entire complex-valued (magnitude and phase) data [49, 50]. The goal in fMRI has been to utilize the phase information in order to suppress or bias against determining voxels as active in terms of task-related phase changes, so as to remove spuriously active voxels that are distant from the site of neuronal activation [29 32].

REMOVAL OF THE VEIN CONTRIBUTION IN fMRI USING PHASE INFORMATION

A subject was imaged using a standard resolution flow compensated SWI sequence (TR/TE = 46/28 ms, flip angle = 20°, voxel size = $0.5 \times 0.7 \times 1\ \text{mm}^3$) at 3 T. A venogram was created by taking a minimum intensity projection (mIP) through several slices [22]. The subject then performed a blocked design visual task of rest/active flickering checkerboard and was scanned with a normal GE-EPI sequence. Activations are computed as described in Ref. 3. Signed z-statistics are generated with an $\alpha = 0.05$ slicewise Bonferroni adjusted threshold.

The results for one slice are presented in Figure 30.7. Figure 30.7a is a mIP venogram through the shown functional slice and its neighboring slices. Figure 30.7b shows the

FIGURE 30.5 *(a) Relative signal change of a cortical (gray matter) region (open diamonds) and of a venous region (solid squares). Insert shows the enlarged signal change of the cortical ROI. (b) Left: 3D projection of the signal change (ΔS) map. Middle: venous mask obtained by including only pixels with $\Delta S > 4.5\%$. Right: ΔS map after applying the venous mask (different scaling). (c) Single slice image of a functional SWI data set acquired at 7 T with an isotropic resolution of 0.75 mm using a surface array (left top). Zoomed region showing a dark stripe (arrows) at the cortical depth of layer 4 (right top). Activation map of the same slice (bottom left) and the corresponding zoomed rectangle showing activation at the site of the stripe (arrows).*

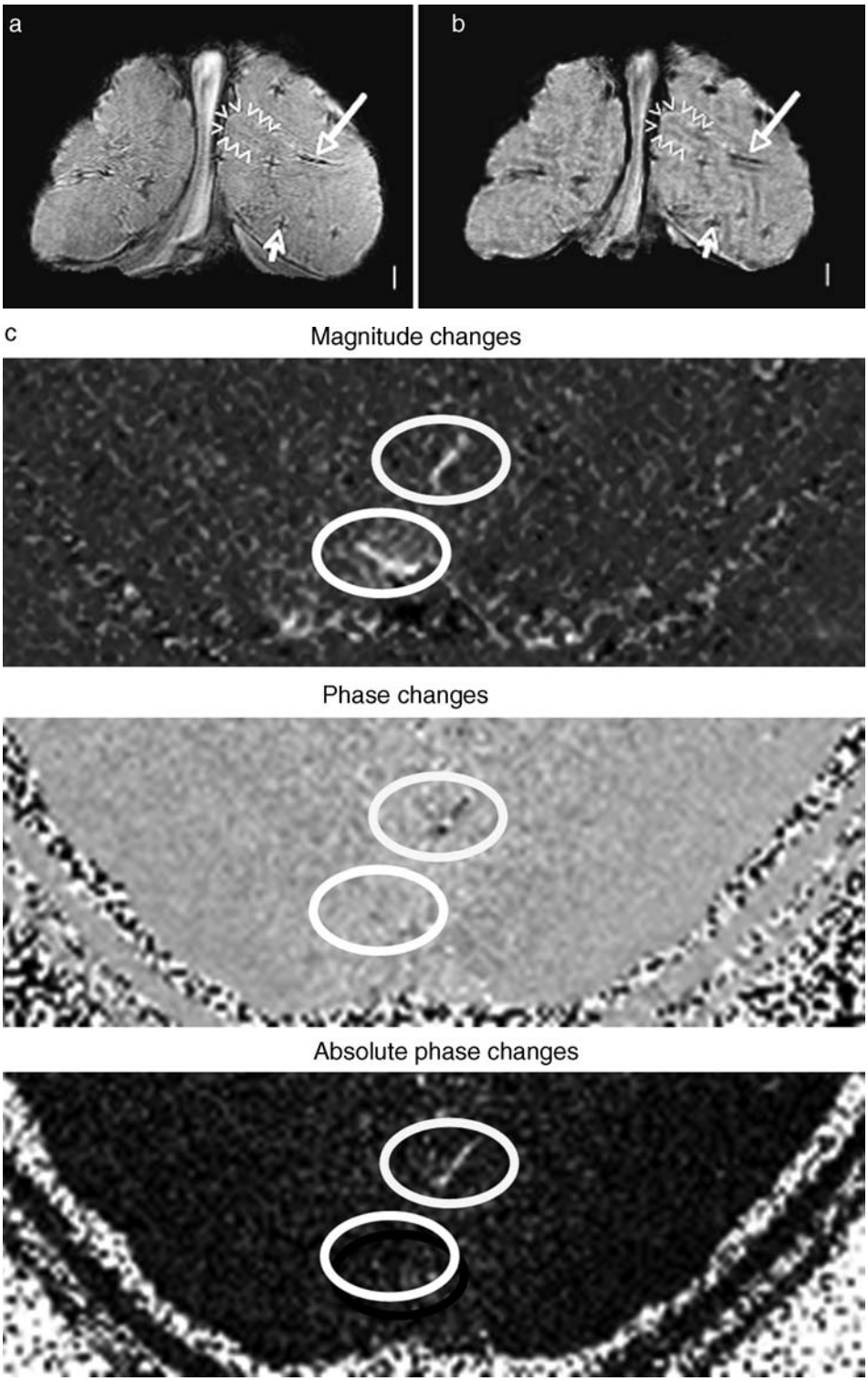
a
b
c
Magnitude changes
Phase changes
Absolute phase changes

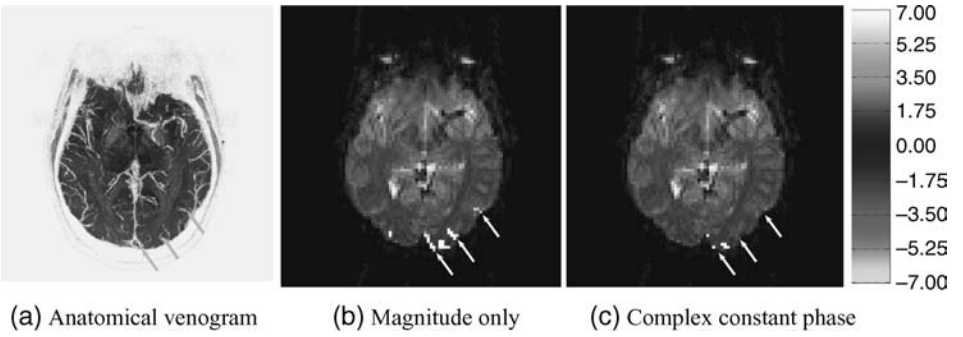

FIGURE 30.7 *(a) Minimum intensity projection of the venogram through the functional slice and its two neighboring slices. (b) Magnitude-only activations from the visual task include regions of activation with a high correspondence to draining veins (arrows). (c) Complex constant phase activations exclude the obvious draining vein activations while preserving a cluster of voxels in which no large draining veins are observed.*

magnitude-only activations, while Figure 30.7c presents the complex constant phase activations. Venous activations are indicated with arrows.

This shows that the phase component of the data can be used to remove or bias against less desirable voxels that contain larger venous vessels. Statistical methods can be successfully utilized to bias against these larger venous vessels. In the simulation on ideal data (results not shown), the complex constant phase model retains the power of the magnitude-only method at low CNRs when little to no task-related phase changes are present, but can bias against determining voxels that have larger TRPCs but low CNR as active. These are favorable properties to an activation model. As the CNR increases, the complex constant phase model will behave more similarly to the magnitude-only model. However, the complex constant phase model may still include some draining vein activations with large CNR and TRPCs. It should also be noted that additional simulations (not shown) have observed that the larger the SNR, the larger the bias against voxels with task-related phase changes. In the experimentally acquired data shown here, the magnitude-only model detects four primary regions of focal activation. Three are identified in the venogram as hypointense areas, denoted by the arrows in Figure 30.7, strongly indicating the existence of large venous structures. The complex constant phase model detects a subset of the magnitude-only activations as has been previously observed [49]. The two of the three activation regions corresponding to hypointense venogram areas are completely eliminated with the complex constant phase model while the third is also nearly eliminated. The single activation region that does not correspond to a hypointense area in the venogram is not eliminated and is strongly believed to be parenchymal in origin.

Moreover, it has been reported that magnitude-only and complex constant phase activations in fMRI data utilizing a spin echo pulse sequence are quite similar [50]. This suggests that the spin echo pulse sequence suppresses the BOLD contributions from large

FIGURE 30.6 *(a) Slice through the occipital cortex showing the cross-shaped pattern around the cross section of small veins (small arrow; resolution: 0.5 mm isotropic, 3 T). Long arrow points to a vein running in-plane. Arrowheads follow the shape of a sulcus. (b) The processed SWI image. (c) Phase changes that accompany magnitude changes in fMRI. From top to bottom: magnitude changes, phase changes, and absolute phase changes.*

veins but retains signal from the capillary bed that has constant phase. Therefore, the complex constant phase model results in similar activation as the magnitude-only model. In addition, the complex constant phase model implemented on a gradient echo image yields results similar to both magnitude and complex constant phase model results on spin echo images. This suggests that the complex constant phase model biases against the BOLD activations from larger venous vessels and returns those from the parenchymal capillary bed. In the meantime, the strong correlation of magnitude-only BOLD activations with large draining veins is in agreement with many studies [51].

It is also possible that reduction in non-task-related phase changes is responsible for the decreased volume of parenchymal activation found by the complex constant phase method. This could also be the result of unresolved, well-oriented draining veins within the volume. It should also be noted that a parallel line of research aiming at direct detection of magnetic field changes due to neuronal activation has tried to utilize the time series of phase in addition to the magnitude. At present, magnetic field changes in wire phantoms have been detected [52] while human results are not yet conclusive [53].

To conclude, the biological information contained in the phase of MR data can be used to increase the functional specificity of fMRI activation to the parenchymal tissue [54]. In the future, the use of the phase should become regular practice in MR imaging.

REFERENCES

1. Ogawa S, Lee TM, Kay AR, Tank DW. Brain magnetic resonance imaging with contrast dependent on blood oxygenation. *Proc. Natl. Acad. Sci. USA* 1990;87:9868 9872.
2. Ogawa S, Lee TM, Nayak AS, Glynn P. Oxygenation sensitive contrast in magnetic resonance image of rodent brain at high magnetic fields. *Magn. Reson. Med.* 1990;14:68 78.
3. Bandettini PA, Jesmanowicz A, Wong EC, Hyde JS. Processing strategies for time course data sets in functional MRI of the human brain. *Magn. Reson. Med.* 1993;30:161 173.
4. Hoge RD, Atkinson J, Gill B, Crelier GR, Marrett S, Pike GB. Investigation of BOLD signal dependence on cerebral blood flow and oxygen consumption: the deoxyhemoglobin dilution model. *Magn. Reson. Med.* 1999;42:849 863.
5. Grubb RL, Jr., Raichle ME, Eichling JO, Ter Pogossian MM. The effects of changes in $PaCO_2$ on cerebral blood volume, blood flow, and vascular mean transit time. *Stroke* 1974;5:630 639.
6. van Zijl PC, Eleff SM, Ulatowski JA, Oja JM, Ulug AM, Traystman RJ, Kauppinen RA. Quantitative assessment of blood flow, blood volume and blood oxygenation effects in functional magnetic resonance imaging. *Nat. Med.* 1998;4:159 167.
7. Lai S, Hopkins AL, Haacke EM, Li D, Wasserman BA, Buckley P, Friedman L, Meltzer H, Hedera P, Friedland R. Identification of vascular structures as a major source of signal contrast in high resolution 2D and 3D functional activation imaging of the motor cortex at 1.5T: preliminary results. *Magn. Reson. Med.* 1993;30:387 392.
8. Frahm J, Merboldt KD, Hanicke W, Kleinschmidt A, Boecker H. Brain or vein oxygenation or flow? On signal physiology in functional MRI of human brain activation. *NMR Biomed.* 1994;7:45 53.
9. Segebarth C, Belle V, Delon C, Massarelli R, Decety J, Le Bas JF, Decorps M, Benabid, AL. Functional MRI of the human brain: predominance of signals from extracerebral veins. *Neurore port* 1994;5:813 816.

10. Barth M, Reichenbach JR, Venkatesan R, Moser E, Haacke EM. High resolution, multiple gradient echo functional MRI at 1.5 T. *Magn. Reson. Imaging* 1999;17:321 329.
11. Hoogenraad FG, Hofman MB, Pouwels PJ, Reichenbach JR, Rombouts SA, Haacke, EM. Sub millimeter fMRI at 1.5 Tesla: correlation of high resolution with low resolution measurements. *J. Magn. Reson. Imaging* 1999;9:475 482.
12. Hoogenraad FG, Pouwels PJ, Hofman MB, Reichenbach JR, Sprenger M, Haacke EM. Quantitative differentiation between BOLD models in fMRI. *Magn. Reson. Med.* 2001;45:233 246.
13. Barth M, Norris DG. Very high resolution three dimensional functional MRI of the human visual cortex with elimination of large venous vessels. *NMR Biomed.* 2007;20:477 484.
14. Oja JM, Gillen J, Kauppinen RA, Kraut M, van Zijl PC. Venous blood effects in spin echo fMRI of human brain. *Magn. Reson. Med.* 1999;42:617 626.
15. Ugurbil K, Hu X, Chen W, Zhu XH, Kim SG, Georgopoulos A. Functional mapping in the human brain using high magnetic fields. *Phil. R. Soc. Lond.* B 1999;354:1195 1123
16. Duvernoy HM, Delon S, Vannson JL. Cortical blood vessels of the human brain. *Brain Res. Bull.* 1981;7:519 579.
17. Yamaguchi S, Yamakawa T, Niimi H. Red cell velocity and microvessel diameter measurement by a two fluorescent tracer method under epifluorescence microscopy: application to cerebral microvessels of cats. *Int. J. Microcirc. Clin. Exp.* 1992;11:403 416.
18. Koopmans PJ, Barth M, Norris DG. Layer specific BOLD activation in human V1. Hum Brain Mapp. 2010 Sep;31(9):1297 304.
19. Turner R. How much cortex can a vein drain? Downstream dilution of activation related cerebral blood oxygenation changes. *Neuroimage* 2002;16:1062 1067.
20. Lauwers F, Cassot F, Lauwers Cances V, Puwanarajah P, Duvernoy H. Morphometry of the human cerebral cortex microcirculation: general characteristics and space related profiles. *Neuroimage* 2008;39:936 948.
21. Boxerman JL, Bandettini PA, Kwong KK, Baker JR, Davis TL, Rosen BR, Weisskoff RM. The intravascular contribution to fMRI signal change: Monte Carlo modeling and diffusion weighted studies *in vivo*. *Magn. Reson. Med.* 1995;34:4 10.
22. Reichenbach JR, Venkatesan R, Schillinger DJ, Kido DK, Haacke EM. Small vessels in the human brain: MR venography with deoxyhemoglobin as an intrinsic contrast agent. *Radiology* 1997;204:272 277.
23. Reichenbach JR, Barth M, Haacke EM, Klarhofer M, Kaiser WA, Moser E. High resolution MR venography at 3.0 Tesla. *J. Comput. Assist. Tomogr.* 2000;24:949 957.
24. Dashner RA, Clark DL, Kangarlu A, Baudendistel KT, Chakeres DW. Epoxy resin injection of the cerebral arterial microvasculature: an evaluation of the limits of spatial resolution in 8 Tesla MRI. *Clin. Anat.* 2005;18:164 170.
25. Gati JS, Menon RS, Ugurbil K, Rutt BK. Experimental determination of the BOLD field strength dependence in vessels and tissue. *Magn. Reson. Med.* 1997;38:296 302.
26. Barth M, Reichenbach JR, Venkatesan R, Moser E, Haacke EM. High resolution, multiple gradient echo functional MRI at 1.5 T. Magn Reson Imaging. 1999;17:321 9.
27. Yacoub E, Van De Moortele PF, Shmuel A, Ugurbil K. Signal and noise characteristics of Hahn SE and GE BOLD fMRI at 7 T in humans. *Neuroimage* 2005;24:738 750.
28. Cheng K, Waggoner RA, Tanaka K. Human ocular dominance columns as revealed by high field functional magnetic resonance imaging. *Neuron* 2001;32:359 374.
29. Menon RS. Postacquisition suppression of large vessel BOLD signals in high resolution fMRI. *Magn. Reson. Med.* 2002;47:1 9.

30. Rowe DB. Modeling both the magnitude and phase of complex valued fMRI data. *Neuroimage* 2005;25:1310 1324.
31. Rowe DB, Nencka AS. Complex activation suppresses venous BOLD in GE EPI fMRI data. *Proc. Intl. Soc. Magn. Reson. Med.* 2006;14:2834.
32. Nencka AS, Rowe DB. Reducing the unwanted draining vein BOLD contribution in fMRI with statistical post processing methods. *Neuroimage* 2007;37:177 188.
33. Song AW, Wong EC, Tan SG, Hyde JS. Diffusion weighted fMRI at 1.5 T. *Magn. Reson. Med.* 1996;35:155 158.
34. Jochimsen TH, Norris DG, Mildner T, Moller HE. Quantifying the intra and extravascular contributions to spin echo fMRI at 3 T. *Magn. Reson. Med.* 2004;52:724 732.
35. Michelich CR, Song AW, Macfall JR. Dependence of gradient echo and spin echo BOLD fMRI at 4 T on diffusion weighting. *NMR Biomed.* 2006;19:566 572.
36. FSL, FMRIB, Oxford, UK. http://www.fmrib.ox.ac.uk/fsl.
37. Reichenbach JR, Essig M, Haacke EM, Lee BC, Przetak C, Kaiser WA, Schad LR. Highresolution venography of the brain using magnetic resonance imaging. MAGMA 1998;6:62 69.
38. Reichenbach JR, Haacke EM. High resolution BOLD venographic imaging: a window into brain function. NMR Biomed. 2001;14:453 467.
39. Koopmans PJ, Manniesing R, Norris DG,Viergever M, Niessen WJ, Barth M. MR venography of the human brain using susceptibility weighted imaging at very high field strength. Magn Reson Mater Phys (MagMa) 2008;21: 149 158.
40. Cusack R, Mitchell DJ, Beauregard DA, Salfity MF, Huntley JM. Individual variability in cerebral vein structure and the BOLD signal. In: Proceedings of the Organization for Human Brain Mapping, Florence, Italy, 2006, S99.
41. Zhao F, Jin T, Wang P, Hu X, Kim SG. Sources of phase changes in BOLD and CBV weighted fMRI. *Magn. Reson. Med.* 2007;57:520 527.
42. Sedlacik J, Kutschbach C, Rauscher A, Deistung A, Reichenbach JR. Investigation of the influence of carbon dioxide concentrations on cerebral physiology by susceptibility weighted magnetic resonance imaging (SWI). *Neuroimage* 2008;43:36 43.
43. Duyn, JH, van Gelderen, P, Li T Q, de Zewart JA, Koretsky AP, Fukunaga M. High field MRI of brain cortical substructure based on signal phase. *PNAS* 2007;104:11796 11801.
44. Hoogenraad FG, Reichenbach JR, Haacke EM, Lai S, Kuppusamy K, Sprenger M. *In vivo* measurement of changes in venous blood oxygenation with high resolution functional MRI at 0.95 Tesla by measuring changes in susceptibility and velocity. *Magn. Reson. Med.* 1998;39:97 107.
45. Springer CS, Xu Y. Aspects of bulk magnetic susceptibility in *in vivo* MRI and MRS. In: Rink PA, Muller, RN, editors. *New Developments in Contrast Agent Research*, European Magnetic Resonance Forum, Blonay, Switzerland, 1991, pp. 13 25.
46. Weisskoff RM, Kiihne S. MRI susceptometry: image based measurement of absolute suscep tibility of MR contrast agent and human blood. *Magn. Reson. Med.* 1992;24:375 383.
47. Guyton AC. *Textbook of Medical Physiology*, W.B. Saunders Company, Philadelphia, PA, 1981, p. 206.
48. Pfeuffer J, Van de Moortele PF, Ugurbil K, Hu X, Glover GH. Correction of physiologically induced global off resonance effects in dynamic echo planar and spiral functional imaging. *Magn. Reson. Med.* 2002;47:344 353.
49. Rowe DB, Logan BR. A complex way to compute fMRI activation. *Neuroimage* 2004;23:1078 1092.
50. Nencka AS, Rowe DB. Complex constant phase method removes venous BOLD component in fMRI. *Proc. Intl. Soc. Magn. Reson. Med.* 2005;13:495.

51. Duong TQ, Yacoub E, Adriany G, Hu X, Uurbil K, Kim S G. Microvascular BOLD contribution at 4 and 7 T in the human brain: gradient echo and spin echo fMRI with suppression of blood effects. *Magn. Reson. Med.* 2003;49:1019 1027.

52. Bodurka J, Jesmanowicz A, Hyde JS, Xu H, Estkowski L, Li S J. Current induced magnetic resonance phase imaging. *J. Magn. Reson.* 1999;137:265 271.

53. Bandettini PA, Petridou N, Bodurka J. Direct detection of neuronal activity with MRI: fantasy, possibility, or reality? *Appl. Magn. Reson.* 2005;29:65 88.

54. Rowe DB. Complex activation is more focal and concentrated to parenchymal tissue. *Proc. Intl. Soc. Magn. Reson. Med.* 2005;13:1575.